Journal of The Korea Society of Computer and Information
Vol. 17, No. 12, December 2012
www.ksci.re.kr
http://dx.doi.org/10.9708/jksci/2012.17.12.101

서포트 벡터와 뱀형상 윤곽선을 이용한 TRUS 영상의 전립선 분할

박재홍*, 서영건*

A Prostate Segmentation of TRUS Image using Support Vectors and Snake-like Contour

Jae Heung Park*, Yeong Geon Seo*

요 약

TRUS 영상에서 전립선에 대한 많은 진단과 치료 과정에서 정확한 전립선 경계의 추출이 요구된다. 여기에는 전립선 경계의 애매함, 반점, 낮은 그레이 레벨로 인하여 많은 어려움이 존재한다. 본 논문에서는 서포트 벡터와 뱀형상 윤곽선을 이용하여 TRUS 영상의 자동 전립선 분할에 대한 방법을 제안한다. 이 방법은 전처리, 가버 특성 추출, 학습, 전립선 추출 단계로 구성된다. 텍스처 특성을 추출하기 위하여 가버 필터 뱅크가 사용되며, 학습 과정에서 전립선과 비전립선의 각 특성을 얻기 위하여, SVM이 사용된다. 전립선의 경계는 뱀형상 윤곽 알고리즘에 의해 추출된다. 실험 결과, 제안된 알고리즘은 인간 전문가가 추출한 경계와 비교했을 때 9.3%보다 적은 차이로 전립선 경계를 추출할 수 있었다.

▸ Keywords : 서포트 벡터, 뱀형상윤곽, TRUS, 전립선

Abstract

In many diagnostic and treatment procedures for prostate disease accurate detection of prostate boundaries in transrectal ultrasound(TRUS) images is required. This is a challenging and difficult task due to weak prostate boundaries, speckle noise and the short range of gray levels. In this paper a method for automatic prostate segmentation in TRUS images using support vectors and snake-like contour is presented. This method involves preprocessing, extracting Gabor feature, training, and prostate segmentation. Gabor filter bank for extracting the texture features has been implemented. A support vector machine(SVM) for training step has been used to get each feature of prostate and

• 제1저자 : 박재홍 • 교신저자 : 서영건
• 투고일 : 2012. 10. 29 심사일 : 2012. 10. 30 게재확정일 : 2012. 11. 1
* 경상대학교 컴퓨터과학과, 컴·정보통신연구원 (Dept. of Computer Science, Gyeongsang National Univ.)

nonprostate. The boundary of prostate is extracted by the snake-like contour algorithm. The results showed that this new algorithm extracted the prostate boundary with less than 9.3% relative to boundary provided manually by experts.

▸ Keywords : Support Vector, Snake-like Contour, TRUS, Prostate

Ⅰ. Introduction

According to the American Cancer Society, dead rate is decreasing every year caused by prostate cancer, but it is 23 per 100,000 people in 2007[1-3]. The rate is second highest value following the dead rate of lung and bronchus. Hence diagnosis of the cancer of the early stages is crucial. Ultrasound imaging is a widely used technology for diagnosing and treatment this kind of cancer [4]. Especially, prostate transrectal ultrasound (TRUS) prostate images are captured easier and with lower cost. In fig. 1, an example of TRUS image capture is shown. US imaging is the main modality for prostate cancer diagnosis and treatment, due to many of its clinical advantages, expensive and easy to use. Accurate segmentation of prostate boundaries from US images plays an important role in many prostate-related applications such as the accurate placement of the needles and biopsy, the assignment of the appropriate therapy in cancer treatment, and the measurement of the prostate gland volume [5]. Moreover, the shape of the prostate in US images is considered as an important indicator for staging prostate cancer. But, because the boundaries between prostate and nonprostate of the image are ambiguous, an automatic extraction of the boundaries has some difficulties [6,7]. Such that, they are very weak texture structure, low contrast, fuzzy boundaries, speckle noise and shadow regions.

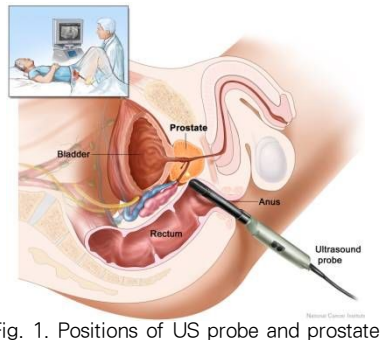

Fig. 1. Positions of US probe and prostate

Shen developed a deformable segmentation using Gabor-SVM based 3D prostate images [6]. Pathak presented a new paradigm for the edge guided delineation, providing the algorithm detected prostate edges as a visual guidance for the user to manually edit [8]. Shen designed a statistical shape model for outlining prostate boundary from 2D TRUS images [9]. Shao presented a level set based method to detect prostate surface from 3D US images [10]. Yan proposed an automatic segmentation for the prostate from 2D TRUS using adaptive learning local shape statistics [11]. Akbari presented an automatic segmentation of the prostate in 3D TRUS images by extracting texture features and by statistically matching geometrical shape of the prostate [12].

This paper consists of preprocessing, extracting Gabor feature which extracts and characterizes texture features in US images using Gabor filters at multiscales and multiorientations. training which trains the Gabor texture features using SVM and each pixel of the test image is classified to prostate or nonprostate. The final step applies snake-like algorithm and gets the smooth boundaries between

them. The results experimented from our method made difference by 9.3% compared to one of human expert.

II. Related Studies

In this chapter, we present Gabor transform, SVM and deformable segmentation.

2.1 Gabor Transform

The Gabor transform, named after Dennis Gabor, is a special case of the short-time Fourier transform. It is used to determine the sinusoidal frequency and phase content of local sections of a signal as it changes over time. The function to be transformed is first multiplied by a Gaussian function, which can be regarded as a window, and the resulting function is then transformed with a Fourier transform to derive the time-frequency analysis. The window function means that the signal near the time being analyzed will have higher weight. The Gabor transform of a signal x(t) is defined by this formula.

$$G_x(t,f) = \int_{-\infty}^{\infty} e^{-\pi(\tau-t)^2} e^{-j2\pi f\tau} x(\tau) d\tau$$

The Gaussian function has infinite range and it is impractical for implementation. But take a look at the distribution of Gaussian function.

$$\begin{cases} e^{-\pi a^2} \geq 0.00001; & |a| \leq 1.9143 \\ e^{-\pi a^2} < 0.00001; & |a| > 1.9143 \end{cases}$$

Gaussian function with |a|>1.9143 can be regarded as 0 and also can be ignored. Here, a is time(sec). Thus the Gabor transform can be simplified as

$$G_x(t,f) = \int_{-1.9143}^{1.9143} e^{-\pi(\tau-t)^2} e^{-j2\pi f\tau} x(\tau) d\tau$$

This simplification makes the Gabor transform practical and realizable. Here, τ is window time at the center of window. The Gabor transform is invertible. The original signal can be recovered by the following equation.

$$x(t) = \int_{-\infty}^{\infty} G_x(t,f) e^{j2\pi tf} df$$

2.2 SVM

The standard SVM takes a set of input data and predicts, for each given input, which of two possible classes comprises the input, making the SVM a non-probabilistic binary linear classifier. Given a set of training examples, each marked as belonging to one of two categories, an SVM training algorithm builds a model that assigns new examples into one category or the other. The original optimal hyperplane algorithm proposed by Vapnik was a linear classifier. Linear SVM gives some training data D, a set of n points of the form.

$$D = \{(x_i, y_i) \mid x_i \in R^p,\ y_i \in \{-1, 1\}\}_{i=1}^{n}$$

where the yi is either 1 or −1, indicating the class to which the point xi belongs. Each xi is a p-dimensional real vector. We want to find the maximum-margin hyperplane that divides the points having yi=1 from those having yi=-1.

In 1992, Vapnik suggested a way to create nonlinear classifiers by applying the kernel trick to maximum-margin hyperplanes [13]. The resulting algorithm is formally similar, except that every dot product is replaced by a nonlinear kernel function. This allows the algorithm to fit the maximum-margin hyperplane in a transformed feature space. The transformation may be nonlinear and the transformed space high dimensional; thus though the classifier is a hyperplane in the high-dimensional feature space, it may be nonlinear in the original input space. Fig. 2 shows an example of linear and nonlinear SVM, respectively.

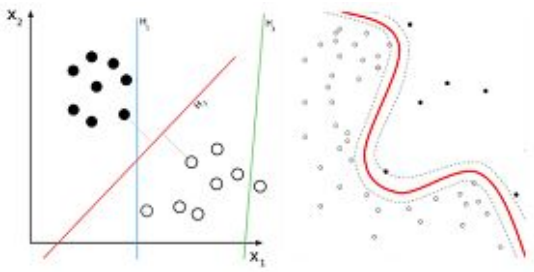

Fig. 2. Linear SVM and nonlinear SVM

2.3 Deformable Segmentation

Deformable models are curves or surfaces defined in an image. They are physically motivated model-based techniques for delineating region boundaries by fitting closed parametric curves or surfaces to image data by means of energy minimization. Those models deform under the influence of two basic components of an energy function. The two components are the internal and external forces as following equation.

$$E = E_{ext} + aE_{int}$$

The process of deformation is performed by minimizing the energy function, E, that is designed in such a way that its local minimum is obtained at the boundary of the object. The external energy Eext derives the mesh towards the surface patches obtained in the surface detection step. The internal energy Eint restricts the flexibility of the mesh. The parameter aweights the relative influence of each term.

There are two types of deformable models described in the literature, parametric deformable models and level set-based deformable models [14]. Parametric models have gained significant attention throughout the image processing. These models have been used in edge detection, object recognition, shape modeling, and motion tracking.

For example, Zhan used deformable surface model and divided the whole temporary boundaries to several areas, subsurface [6]. Energy function evaluates the matching degree and defines two energy terms on each vertex $\overrightarrow{P_i}$ of the surface model. Internal energy is defined by the geometric attribute vectors and used to preserve the geometric regulation. External energy is defined by texture-based tissue labeling results and used to drive the deformable model to the boundary. Texture-based external energy on $\overrightarrow{P_i}$ of jth subsurface is

$$E^{EXT}(\overrightarrow{P_i}) = w_{sum}E_{sum}(\overrightarrow{P_i}) + w_{DIST}E_{DIST}(\overrightarrow{P_i})$$

$$E_{sum}(\overrightarrow{P_i}) = \left(\left(\frac{\Sigma_{\forall \vec{v} \in N(\overrightarrow{P_i})} L(\vec{v};j)}{\Sigma_{\forall \vec{v} \in N(\overrightarrow{P_i})} 1} \right) - 0.5 \right)^2$$

$$E_{DIST}(\overrightarrow{P_i}) = \frac{(d(\overrightarrow{C_p}, \overrightarrow{P_i}) - d(\overrightarrow{C_{NP}}, \overrightarrow{P_i}))^2}{R^2}$$

Here, N(.) : spherical neighborhood with the radius R, around $\overrightarrow{P_i}$. d(.,.) : 3D Euclidean distance. $\overrightarrow{C_P}$, $\overrightarrow{C_{NP}}$: centers of the prostate voxels, i.e., $\{\vec{v} | L(\vec{v};j) \geq 0.5\}$, and the nonprostate voxels, i.e., $\{\vec{v} | L(\vec{v};j) < 0.5\}$, respectively.

III. Segmentation using Gabor Features and Snake-like Contour

The method consists of preprocessing, Gabor feature extraction, training and application steps. The steps excluding application step are repeated several times as the training images.

3.1 Preprocessing

Histogram equalization enhances the contrast of images by transforming the values in an intensity image, so that the histogram of the output approximately matches a specified histogram. Stick filtering filters to reduce the speckle noise. Morphological filtering is used to smooth filtered image and enhanced contrast near edges. Final step

gets background and probe which will be used to be excluded for training.

Histogram equalization considers a discrete gray scale image, x, and lets n ibe the number of occurrences of gray level, i. The probability of an occurrence of a pixel level, i in the image is

$$p_x(i) = p(x = i) = \frac{n_i}{n}, 0 \le i < L$$

Here, L is the total number of gray levels in the image, n is the total number of pixels in the image, and px(i) is in fact the image's histogram for pixel value i. The stick filtering algorithm challenges the problem of filtering speckle in US images without losing edge detail. The stick filter determines the mean of neighboring pixels in the direction of the stick - the most likely direction of the linear feature passing through (x,y). If n is the stick's length, there are 2*n-2 possible orientations. We use 5 length pixels as fig. 3.

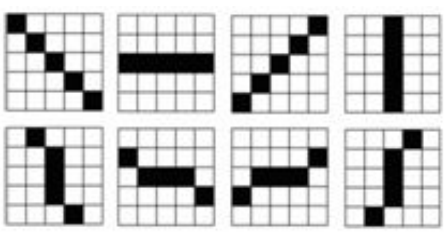

Fig. 3. Stick filters of five length pixels

In morphological filtering, the top-hat and bottom transformation are applied on output of stick filter (Fs) with using an ordinary neighborhood window. We use a disk with radius 3 in top-hat, bottom-hat transformation.

Ht= top − hat(Fs)
Hb= bot - hat(Fs)
Fp= Fs+ Ht− Hb

Ht is the top-hat and Hb is the bottom-hat transformation and Fp is the preprocessed image. We get background and probe, and then exclude them in step of training. Generally the background is black and is apparently unusable region. The probe which is generally an exploring needle in fig. 1, but is a half circle shaped black region that is useless region as well.

3.2 Extracting Gabor texture features

Gabor filter bank is obtained by the dilation and rotation of the mother function. Here, we use that total numbers of the orientations are K=4, the scale numbers of the scales are S=2. So the basic rotation and scale factors are ψ=π/K and a=(Uh/Ul)1/S-1 respectively. Uh and Ul are parameters that determine the frequency range of the Gabor filter bank. We use Uh=0.1 and Ul=0.025. Using the scale variables and the rotation variables, the (s,k)th Gabor filter is

$$g_{s,k}(x,y) = a^s g(a^s(x\cos(k\psi)+y\sin(k\psi))a^s(-x\sin(k\psi)+y\cos(k\psi)))$$

The Gabor filter bank has two important properties, the frequency spectrum of the filter bank has a multiscale and multiorientation structure and each filter can be separated into two parts, i.e., the real part and the imaginary part. The real part is regarded as a smooth filter and the imaginary part is done as an edge detection filter. Using Gabor filter bank offers three advantages. First, it can smooth the image and remove speckle noises. Second, the multiscale structure enables hierarchical implementation. Third, the multiorientation structure enables the extractions of edge direction, edge strength and rotation-invariant features. Fig. 4 shows 2D Gabor filter bank used in the proposed method. First rows are S=1 and second rows are S=2. First columns are K=1, second ones are K=2, third ones are K=3, and last ones are K=4.

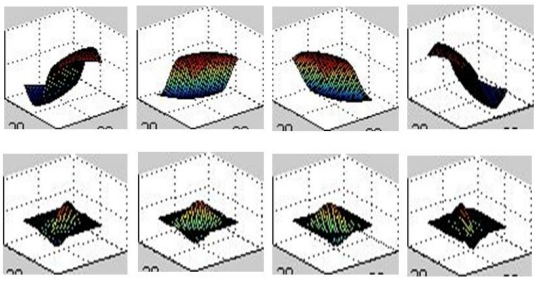

Fig. 4. 2D Gabor filter banks

All the features are the imaginary parts. The values of the features are normalized to 0-255 for display purposes. Here, it can use a number of orientations and scales, but they can generate tons of data. Also, it can use the real part Gabor features. So the proper negotiation is needed. In this paper, we use 8 Gabor texture features per pixel which consist of K=4, S=2 and the imaginary part Gabor features.

3.3 Training the Gabor features

Each pixel should be classified to prostate or nonprostate whether each pixel belongs to which region using SVM. To classify the region, the human expert is needed. The inner part of the contours drawn by the expert is prostate and the outside of the contours is nonprostate. The pixels around the contour acquired from the expert and the useless region are excluded in the training process. Why the pixels around the contour are excluded is that they don't have classifiable features comparing to other regions. Next, each pixel has 8 Gabor features which will be trained and have the following input format.

```
-1 1:33.248316   2:34.518724   3:19.255745
   4:4.296715    5:33.996764   6:35.103513
   7:19.049476   8:3.813344
 1 1:-5.961116   2:-1.852036   3:2.131680
   4:4.366701    5:-6.335777   6:-1.963415
   7:1.260157    8:3.865562
```

First columns, -1 and 1 mean nonprostate and prostate, respectively. The numbers from 1 to 8 mean each pixel's Gabor feature orders that the first 4 features (1-4) are S=1 and K=1, 2, 3, and 4, and the next 4 ones (5-8) are S=2 and K=1, 2, 3, and 4, in the order named. The real numbers are the values of Gabor texture feature. After training the features, a number of support vectors and their coefficients are acquired.

3.4 Dividing the pixels to prostate and nonprostate

The input format for predicting whether each pixel belongs to prostate or nonprostate is same as one of training step. But here all the pixels are tested without excluding any pixel. The results from prediction have -1 or 1, nonprostate or prostate, respectively. Fig. 5 shows a test image its labels which the black ones are nonprostate, and the white ones are prostate.

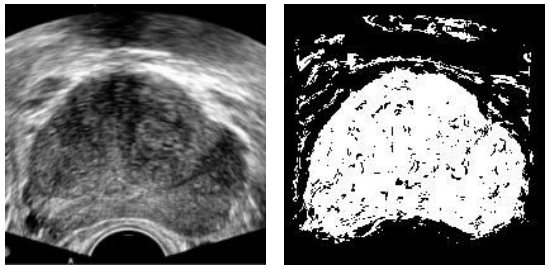

Fig. 5. A test image and its predicted labels

First of all, wrong classified pixels are needed to be excluded from the labels. The algorithm to exclude the noise pixels is simple. The pixels not included in one big white label and the pixels not included in one big black label may be only excluded as shown in (a) of fig. 6. After removing noises, the contour has rough line around meeting the prostate and non prostate. Real prostate boundary doesn't have protrusion, so protrusions need to be removed. We use 7x7 mask to find a block that one side is opened and the other three sides are closed in different sides. The result after removing the protrusions and smoothing with radius=30 is shown in (b) of fig. 6.

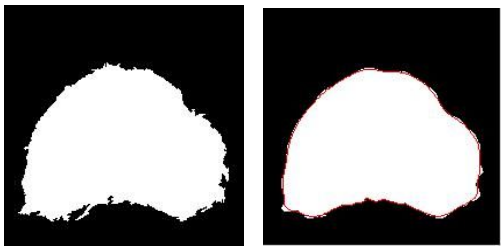

Fig. 6. (a) Labels after excluding wrong classified labels (b) Labels after removing protrusion and smoothing with radius = 30

3.5 Smoothing the contours

In a simple 2D point set or a curve the points do not have to line in a specific order. The contour smoothing is done by projecting all the contour points onto the local regression line. For each point, N neighboring points which lie on the contour are sampled on each side and a local regression line is computed. Then the current point is projected on this line. Applying this algorithm to all the points smooths the contour and in a way brings the points closer. 2N+1 is the number of total points contributing to the computation of the local regression line. The higher the number of point is, the smoother the curve is. Because of the linear nature of fitting, when too much smoothing is desired, some important features such as protrusions may be loosed. This in a way is a wrong over-smoothing. A way to be less prone to such errors is to use Gaussian weighted least squares fit. To do this, the algorithm is the following and the labels after smoothing with radius = 30 shows in fig. 6 (b).

- Converts 2D contours to chain code, a vector for x positions and a vector for y positions.
- Get maximum and minimum values of X, Y.
- For all the points, (Xi, Yi) with radius (=30 or 20)
  . get (radius*2+1) points in the middle of a point from the chain code.
  . compute the weighted orthogonal least square value of the points
  . project point(Xi, Yi) on local regression line defined as the value and get new values, X2, Y2
  . X2, Y2 values should be inside X, Y
- New values, X2, Y2 are the smoothed contours

IV. Experiment and Evaluation

4.1 Classifying pixels from support vectors

SVM was used to predict whether each pixel is prostate or nonprostate using the training model. Fig. 7 shows testing images, their predicting labels, and labels after removing the island labels, which the white labels are predicted as prostate and the black labels as nonprostate. The reason the white labels are distributed in the black labels is why the texture features of them are similar, so removing the island labels is needed.

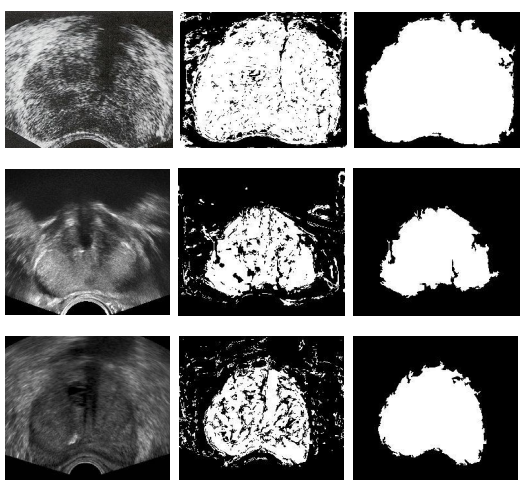

(a) (b) (c)

Fig. 7. (a) Sample images (b) classified labels (c) labels after removing ithe slands

4.2 Objective and subjective evaluations

The boundaries by human expert and the proposed method are very similar but not same in fig 8. Actually, even human experts have differences of their drawn boundaries. In the figure, the solid line is the delineating boundaries by the proposed

method and the dashed line is one by human expert. For subjective comparison, we used difference between two boundaries. In this paper, we can use radius = 20 or 30, however, the figure shows radius = 30. The difference (D) comes from the following equation.

D = count(for all pixels E(x, y) and P(x,y), labels(E(x,y) != P(x,y))) / count(prostate of E)

Here, E means expert, P means the proposed method. Table 1 shows D for each testing image. Although the difference between the boundaries of human expert and the proposed method is bigger than other test images, D is not too big because the size of the prostate is occupying the big region. The value, 0.095, means that 9.5% labels are wrong classified. The wrong classified labels are distributed on the boundary of prostate and nonprostate.

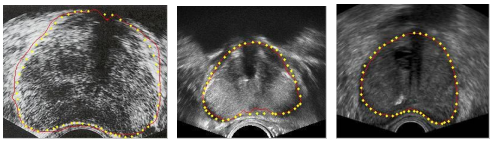

Fig. 8. Delineating boundaries by expert (dashed yellow line) and the proposed one (solid red line)

Table 1. Differences of the boundaries between human expert and the proposed methid

test images \ radius	20	30
image 1	0.095	0.094
image 2	0.093	0.092
image 3	0.094	0.091

V. Conclusion and Future works

This paper proposed a TRUS prostate segmentation using Gabor texture features, SVM, and snake-like contour smoothing algorithm. As the boundary between prostate and nonprostate is not clear and even the textures of them are hard to classify, especially for US prostate image. The proposed method through these processing has difference about 9.3% compared to human expert's contours. Our future studies is to improve the computation time, to apply human expert's knowledge, and finally to implement 3D segmentation.

References

[1] Cancer Facts and Figures. American Cancer Society.

[2] Mettlin C: American society national cancer detection project. Cancer 1995, 75:1790-1794.

[3]http://www.cancer.org/Research/CancerFacts Figures/CancerFactsFigures/cancer-facts-figures-2011

[4] A. Chakraborty, L. H. Staib, and J. S. Duncan,"Deformable Boundary Finding in Medical Images by Integrating Gradient and Region Information," IEEE Trans. Med. Imag., Vol. 15, No. 6, pp. 859 - 870, Dec. 1996.

[5] P. D. Grimm, J. C. Balsko, and H. Ragde, "US Guided Transperineal Implantation of Iodine 125 and Palladium 103 for the Treatment of Early Stage Prostate Cancer," Atlas Urol .Clin. No. Amer., Vol. 2, pp. 113 - 125, 1994.

[6] Y. Zhan and D. Shen, "Deformable Segmentation of 3-D US Prostate Images Using Statistical Texture Matching Method," IEEE Trans. on Med. Imag., Vol. 256, pp. 245-255, March 200.

[7] A. Rafiee, A. Salimi, and A. Roostam, "A Novel Prostate Segmentation Algorithm in TRUS Images," World Academy of Science, Eng. and Tech. 45, pp. 120-124, 2008.

[8] S. D. Pathak, V. Chalana, D. R. Haynor, and Y. Kim, "Edge-guided Boundary Delineation in

Prostate US Images," IEEE Trans. Med. Imag., Vol. 19, No. 12, pp. 1211 - 1221, Dec. 2009.
〔9〕 D. Shen, Y. Zhan, and C. Davatzikos, "Segmentation Prostate Boundaries from Ultrasound Images Using Statistical Shape Model," IEEE Trans. Med. Imag., Vol .22, No. 4, pp. 539 - 551, Apr. 2003.
〔10〕 F. Shao, K. V. Ling, and W. S. Ng, "3-D Prostate Surface Detection from Ultrasound Images based on Level Set Method," in Proc. MICCAI 2003, pp. 389 - 396, 2003.
〔11〕 P. Yan, S. Xu, B. Turkbey and J. Kruecker, "Adaptively Learning Local Shape Statistics for Prostate Segmentation in Ultrasound," IEEE Trans. On Bio. Eng., Vol. 58, No. 3, pp. 633-641, Mar. 2011.
〔12〕 H. Akbari, X. Yang, L. Halig and B. Fei, "3D Segmentation of Prostate US Images Using Wavelet Transform," Proc. of SPIE, 2011.
〔13〕 B. E. Boser, I. M. Guyon and V. N. Vapnik. "A Training Algorithm for Optimal Margin Classifiers," In D. Haussler, 5th Annual ACM Workshop on COLT, pp. 144 - 152, 1992.
〔14〕 J. Suri and A. Farag, "Deformable Models2," Springer, pp. 75-94, 2007.
〔15〕 A. Ghanei, H. Zadeh, A. Ratkesicz, and F. Yin, "A 3D Deformable Model for Segmentation of Human Prostate from Ultrasound Image," Med. Phys., Vol. 28, pp. 2147 - 2153. 2001.

저 자 소 개

박 재 흥

1978년 충북대 수학교육과
1989년 중앙대 대학원 전산과(박사)
1983년~현재 경상대 컴퓨터과학과 교수
관심분야 : 소프트웨어 공학, 테스팅, 소프트웨어 신뢰성, Medical Imaging
Email : pjh@gnu.ac.kr

서 영 건

1987년 경상대학교 전산과 학사
1997년 숭실대학교 전산과 박사
1989년~1992년 삼보컴퓨터
1997년~현재 경상대학교 컴퓨터과학과 교수
2001년~현재 경상대학교 컴퓨터정보통신연구소원
2011년~2012년 UNC at Chapel Hill, School of Medicine, Visiting Scholar
관심분야 : Medical Imaging, JPEG2000, Computer Network
Email : young@gnu.ac.kr